A bacterial protein inhibitor of dUTPase disrupts zebrafish embryogenesis through a conserved active-site mechanism

Viktória Perey-Simon[1,2,#], Zoé Sára Tóth[2,3,#], Dániel Dombovári[1,2], Latifa Kazzazy[3,4], Máté Varga[4], Beáta G. Vértessy[1,2], Gergely Nándor Nagy[1,2,*], Kinga Nyíri[1,2,*]

[1] Department of Applied Biotechnology and Food Science, Faculty of Chemical Technology and Biotechnology, Budapest University of Technology and Economics, Műegyetem rkp. 3., H-1111 Budapest, Hungary

[2] Institute of Molecular Life Sciences, HUN-REN Research Centre for Natural Sciences, Magyar tudósok krt 2. H-1117 Budapest, Hungary

[3] Doctoral School of Biology, Institute of Biology, ELTE Eötvös Loránd University, Pázmány Péter sétány 1/A, H-1117 Budapest, Hungary

[4] Department of Genetics, ELTE Eötvös Loránd University, Pázmány Péter sétány 1/C, H-1117 Budapest, Hungary

[#] These authors contributed equally to the work.

* To whom correspondence should be addressed. Email: nagy.gergely.nandor@vbk.bme.hu; nyiri.kinga@vbk.bme.hu.

Keywords: zebrafish embryogenesis, dUTPase, protein inhibitor, nucleotide metabolism, crystal structure

Abstract

Deoxyuridine triphosphatase (dUTPase) is essential for DNA replication fidelity and embryonic development in metazoa, yet whether a protein inhibitor can acutely disrupt dUTPase function in a living vertebrate has not been tested. The *Staphylococcus aureus* Stl protein inhibits diverse dUTPases *in vitro*, but its efficacy in a eukaryotic organism was unknown. We determined the crystal structure of zebrafish dUTPase in complex with the N-terminal Stl fragment to 2.26 Å resolution, revealing conserved active-site engagement and displacement of the C-terminal arm. Biolayer interferometry confirmed low-nanomolar binding affinity with $K_D = 0.7$ nM, and enzyme assays demonstrated ~50% inhibition of zebrafish dUTPase activity at saturating Stl concentrations. These structural and biophysical data establish that Stl forms a tight inhibitory complex with zebrafish dUTPase, prompting us to test whether this interaction can perturb enzyme function *in vivo*. Microinjection of Stl or its point mutant, retaining dUTPase-inhibitory activity but unable to bind DNA, into fertilized zebrafish oocytes reduces embryo survival to ~60% within 48 hours compared to ~90% in controls, demonstrating that lethality depends on dUTPase targeting rather than DNA binding. Accelerated mortality relative to genetic dUTPase knockout indicates that maternally deposited dUTPase supports viability during early cleavage. Stl thus acts as an immediate, proteinaceous dUTPase inhibitor in a living vertebrate, providing a tool to dissect dUTPase function and regulation during embryonic development.

1 Introduction

Maintaining genome integrity depends critically on the strict regulation of intracellular nucleotide pools. Deoxyuridine triphosphatase (dUTPase or DUT) hydrolyzes dUTP to dUMP and pyrophosphate, thereby preventing incorporation of uracil into DNA and providing substrate for thymidylate biosynthesis. DNA polymerases cannot distinguish between dUTP and dTTP, so whether uracil or thymine is incorporated into the genome depends on the cellular ratio of the two nucleotides. By keeping a low dUTP/dTTP ratio in cells, dUTPase plays a central role in ensuring DNA replication fidelity and genome stability [1–4].

Genetic knockout, RNA silencing or interference of dUTPase has proven lethal in all eukaryotic model organisms examined, including *Caenorhabditis elegans* [5], *Trypanosoma brucei* [6], *Drosophila melanogaster* [7], *Arabidopsis thaliana* [8] and *Mus musculus* [9], underscoring the fundamental importance of this enzyme for development and cell viability. In *Danio rerio*, F0 crispant fish generated via CRISPR/Cas9-mediated knockout of the *dut* gene exhibited severe developmental abnormalities and early larval mortality [10], but this approach did not eliminate maternally derived dUTPase, limiting analysis of its function during the earliest embryonic stages. Recent work further suggests that dUTPase essentiality during development may arise via at least two mechanistic routes: a canonical role in controlling dUTP/dTTP balance and uracil misincorporation, and non-canonical roles in mitotic progression that are not fully explained by uracil-DNA repair alone [11].

An alternative to genetic manipulation is the use of protein-based inhibitors, which provide rapid, reversible, and highly specific inhibition of target enzymes. The bacteriophage-encoded uracil DNA glycosylase inhibitor (UGI) binds uracil DNA glycosylase (UNG) with high affinity [12] and has become a widely used molecular tool, for example, as a core component of cytosine base editors [13]. Anti-CRISPR proteins constitute another class of naturally evolved protein inhibitors that target CRISPR nucleases and are increasingly exploited to achieve controlled regulation of genome editing in cells [14]. These examples illustrate how protein inhibitors, originally discovered in phage or bacterial defense systems, can be repurposed as versatile tools to modulate DNA and RNA processing activities in diverse experimental settings.

The Stl repressor protein from *Staphylococcus aureus* pathogenicity islands has emerged as a broad specificity inhibitor of dUTPases, spanning bacteriophages, bacteria, arthropods and vertebrates [15–23]. Structural analyses showed that Stl^{NT}, the N-terminal section of Stl binds

directly in the active site of trimeric dUTPases – a pocket formed at subunit interfaces by five conserved sequence motifs – sterically blocking substrate access [16,19,20,22–24]. Y112 and Y113 residues of Stl were proven to be essential in trimeric phage dUTPase-binding, as their mutation to alanines abolished complex formation [16]. A DNA-binding-deficient Stl, $Stl^{Q40A,N41A}$ (Stl^{AA}) mutant retained dUTPase binding and inhibitory capacity, providing a critical control to separate dUTPase inhibition from any DNA-binding-dependent functions of Stl [16,22,23,25]. Enzyme kinetic analyses demonstrated that wild-type Stl (Stl^{WT}) inhibits a wide range of dUTPases *in vitro* with variable efficiency [15,17–21]. *In vivo*, overexpression of Stl in *Mycobacterium smegmatis* reduced colony-forming ability and increased dUTP levels without markedly altering genomic uracil content, confirming formation of DUT–Stl complexes and indicating that Stl can perturb dUTPase function in living cells[16]. Conversely, dUTPase knockout in this organism leads to increased genomic uracil repair-associated DNA breaks, and lethality [26,27].

Despite these advances, it has not been shown that any proteinaceous dUTPase inhibitor functions effectively in a living vertebrate organism. It therefore remains unclear whether such inhibitors can penetrate complex embryonic environments, form stable complexes with endogenous eukaryotic dUTPase, and exert biologically significant effects *in vivo*. This question is particularly pertinent in systems where maternal gene products dominate during early development. In zebrafish, dUTPase is maternally deposited: dut mRNA and *Dr*DUT protein are already present in unfertilized eggs and remain at stable levels in early embryos [10], and quantitative proteomics identifies DUT as a maternal protein with stable abundance from 0–6 hpf [28]. Till the occurrence of zygotic genome activation (ZGA), which begins at cycle 10 (around 2.75 hpf), maternal gene products dominate early developmental control [29]. More recently, F0 CRISPR screens targeting maternal regulators have demonstrated that such approaches cannot deplete pre-existing maternal proteins, as they only prevent *de novo* zygotic synthesis [30], underscoring the need for complementary strategies to acutely perturb maternal factors.

Here, we address these gaps by using zebrafish as a vertebrate model to test whether Stl can inhibit a eukaryotic dUTPase *in vivo* and perturb early embryogenesis. We show that microinjection of Stl into single-cell embryos induces early lethality and developmental defects. To understand the molecular basis of these *in vivo* effects, we characterize Stl–*Dr*DUT complex formation by thermal unfolding and biolayer interferometry, determine the crystal structure of the *Dr*DUT–Stl^{NT} complex, and assess Stl-mediated inhibition of *Dr*DUT catalytic activity.

Together, these experiments establish Stl as a functional dUTPase inhibitor in a living vertebrate and as a tool for dissecting canonical and potential non-canonical dUTPase roles during vertebrate embryogenesis.

2 Results

2.1 Stl forms thermally stable complexes with DrDUT

To establish the validity of using Stl as a potential inhibitor of dUTPase function in zebrafish, we first produced wild-type Stl (Stl^{WT}) and *Dr*DUT proteins and tested their interaction *in vitro*. In addition to Stl^{WT}, we examined the DNA-binding-deficient Stl^{AA} variant, thereby controlling for any effects attributable to its DNA binding activity, and the crystallizable variant Stl^{NT}. We also utilized an Stl mutant, $Stl^{Y112A,Y113A}$ (Stl^{YAYA}) as a potential negative control, which was already proven to be deficient in binding to trimeric phage dUTPases [16]. The comparison of the above mentioned Stl variants is presented in Fig. S1 and Table S1.

We used differential scanning fluorimetry to assess complex formation between *Dr*DUT and these four Stl variants. Three of these variants (Stl^{WT}, Stl^{NT}, Stl^{AA}) substantially increased the thermal stability of *Dr*DUT, consistent with robust complex formation. The *Dr*DUT-Stl^{WT} displayed a T_m of ~ 57 °C compared to ~ 43 °C for *Dr*DUT and 51 °C for Stl^{WT}, while *Dr*DUT-Stl^{NT} and *Dr*DUT-Stl^{AA} complexes showed T_m values of ~ 60 °C and ~ 57 °C, respectively, relative to 53 °C and 51 °C for the free proteins (Table I, Fig. S2). These pronounced T_m shifts indicate that these three Stl variants form thermally stable complexes with *Dr*DUT under the conditions tested, providing a basis for quantifying binding kinetics and comparing *Dr*DUT–Stl interactions with those of previously characterized human dUTPase. In the case of Stl^{YAYA} –*Dr*DUT mixture two distinct peaks could be detected in the derivative of the thermal unfolding curve, with the T_m representing the individual proteins (~43 °C for *Dr*DUT and ~57 °C for Stl^{YAYA}) and the area of the peak of dUTPase did not decrease compared to the individual sample (Table I, Fig. S2). No peak with a higher T_m value was observed in case of the sample containing both Stl^{YAYA} and *Dr*DUT. Thus, no complex formation was detected between *Dr*DUT and Stl^{YAYA}.

Table I.

2.2 High-affinity nanomolar binding kinetics determined by biolayer interferometry

To define the strength and dynamics of the *Dr*DUT–Stl interaction more precisely, and to compare it with other dUTPases, we performed biolayer interferometry measurements using

biotinylated Avi-tagged Stl^{WT} immobilized on streptavidin biosensors and monitored association–dissociation responses upon exposure to increasing concentrations of *Dr*DUT.

Global kinetic analysis yielded a dissociation constant of approximately 0.7 nM for the Stl^{WT}-*Dr*DUT interaction (Fig. S3), which is the same order of magnitude as the previously reported Stl^{WT}-hDUT affinity (K_D of ca. 0.2 nM)[31], indicating similarly tight binding. However, both the association and dissociation of *Dr*DUT to Stl^{WT} were markedly slower than for hDUT (k_a of $\approx 6.9\times10^4\ M^{-1}s^{-1}$ and $1.5\times10^6\ M^{-1}s^{-1}$; k_{dis} of $\approx 4.9\times10^{-5}\ s^{-1}$ and $2.7\times10^{-4}\ s^{-1}$ for Stl^{WT}-*Dr*DUT and Stl^{WT}-hDUT[31] binding, respectively) (Table II), resulting in comparable overall affinity despite distinct kinetic parameters. By contrast, Stl^{WT} binding to *Mycobacterium tuberculosis* dUTPase (MtDUT) is characterized by a rapid association and an even slower dissociation, giving a picomolar K_D [22](Table II), underscoring species-specific differences in complex formation.

Thus, although *Dr*DUT–Stl binding affinity lies in the low-nanomolar range, the association and dissociation rates differ substantially from those of human and mycobacterial dUTPases, raising the question of how these kinetic properties relate to the observed differences in apparent inhibitory constants and *in vitro* inhibition efficiency.

Table II.

2.3 Stl inhibits *Dr*DUT catalytic activity

We next examined how *Dr*DUT enzymatic activity responds to increasing concentrations of Stl variants Stl^{WT}, Stl^{AA}, and Stl^{NT}, to link the observed binding properties to catalytic inhibition. All of these variants inhibited *Dr*DUT catalytic activity, with inhibition of 49.6 ± 2.5% (Stl^{WT}), 41.5 ± 2.7% (Stl^{AA}), and 35.4 ± 2.8% (Stl^{NT}) at high inhibitor concentration (400 nM) (Fig. 1, Table III). Apparent inhibitory constants determined from quadratic binding fits were in the nanomolar range for these three variants ($K_{i,app}$ = 41.1 ± 5.9 nM for Stl^{WT}, 78.5 ± 13.7 nM for Stl^{AA} and 117.9 ± 28.7 nM for Stl^{NT}), confirming that these variants inhibit *Dr*DUT in a concentration-dependent manner. None of the variants achieved as strong inhibition as that reported for human dUTPase (hDUT) or MtDUT in complex with Stl^{WT} (~ 70% and ~ 82% inhibition at inhibitor concentration of 400 nM , $K_{i,app}$ = 6.7 ± 2.4 nM and 2.0 ± 1.2 nM for hDUT-Stl^{WT} and MtDUT-Stl^{WT}, respectively)[20,22] (Table III). Still these Stl variants function as genuine inhibitors of zebrafish dUTPase under *in vitro* conditions. We also analyzed the effect of Stl^{YAYA} *in vitro* at a concentration of 400 nM, but observed no reduction of DrDUT activity, which is consistent with the result of thermofluorimetric assay showing no complex formation.

Table III.

Figure 1.

2.4 Crystal structure of the *Dr*DUT–Stl^{NT} complex reveals conserved active-site inhibition

To reveal the structural basis of Stl-mediated inhibition of *Dr*DUT, we determined the crystal structure of *Dr*DUT in complex with Stl^{NT} to 2.26 Å resolution (Fig. 2, Table S2). The asymmetric unit contains two *Dr*DUT trimers, each bound by three Stl^{NT} molecules, forming two essentially identical 3:3 heterohexamers (Fig. S4), and represents the first crystal structure of zebrafish dUTPase.

As generally the core of trimeric dUTPases undergo only minor conformational changes upon complex formation with Stl^{NT} [16,22,24], the substructure is predominantly relevant to the unbound enzyme. Comparing the *Dr*DUT trimer to hDUT, their three-dimensional structures are also largely conserved, consistent with their 71% sequence identity (Fig. 2A, Fig. S5).

The primary complex interaction surface involves the Tyr-rich region of Stl^{NT} bound to the active site of *Dr*DUT (Fig. 2C). Stl^{NT} Tyr116 interacts with *Dr*DUT Arg86 and Arg129 of conserved motifs 2 and 4; Tyr112 interacts with motif 3 residues Val101 and Asp103 via H-bonds and Tyr106 via π-π stacking; and Tyr106 binds *Dr*DUT Arg107 of the same motif. Additional polar interactions peripheral to the core active site are formed between Stl^{NT} residues Asn56, Lys103, Asn107, Tyr113 and Leu152 and *Dr*DUT residues Glu145, Glu151, Thr152, Gly111, and Lys92 (Fig. 2C, Table S3). A secondary binding interface is formed by insertion of *Dr*DUT motif 5 Phe159 into an apolar pocket of Stl^{NT} lined by Met25, Ile67, Ile71, Phe91 and Tyr98, stabilised in some subunit pairs by an additional H-bond between the Phe159 main chain and Stl^{NT} Asp95 (Fig. 2D, Table S3). The *Dr*DUT C-terminal arm - which in the Stl-free enzyme closes the substrate-binding pocket - is thus displaced upon Stl^{NT} binding; it is resolved until Phe159 in chain A but only partially visible in the remaining chains, consistent with the known variability of this contact across subunit pairs in other DUT–Stl^{NT} complexes [22,23,24].

The *Dr*DUT–Stl^{NT} structure aligns closely with previously reported trimeric dUTPase–Stl^{NT} complexes (RMSD 0.79–1.48 Å; Fig. S6, Table S4), confirming that the primary Stl–DUT interface, formed by the dUTPase active site and the Tyr-rich segment of Stl^{NT}, is conserved across species. The prominent role of this Tyr-rich segment in dUTPase-binding was further demonstrated by the fact that alanine mutations at Tyr112 and Tyr113 resulted in an Stl variant that failed to bind to Φ11 phage dUTPase *in vitro* [16]. The secondary motif 5 interface is present in hDUT and *Lv*DUT complexes but absent in Φ11 phage DUT and *Mt*DUT complexes, consistent with its proposed role in fine-tuning inhibitory efficiency in eukaryotic hosts. The

surface area of these secondary interfaces is substantially smaller than those of the primary interface (Table S4), thus it might have a minor contribution to the binding affinity. Furthermore, the formation of this secondary interaction site may be transient, as it was proposed by a previous HDX-MS analysis of hDUT-Stl complex formation [20], and given that it cannot be detected in all subunit pairs in the case of hDUT and LvDUT in complex with Stl^{NT} [19,24.] The conservation of both interfaces between zebrafish and human dUTPase is visualized with a side-by-side structural comparison (Fig. 2B–D vs. Fig. 2E–G), underscoring that this inhibitory binding mode is maintained across vertebrate dUTPases.

Moreover, the electrostatic surface analysis of various DUTs in complex with Stl^{NT} further supports the high degree of similarity among the complexes, especially at the active site and its proximity (Fig. S7). The greatest difference is displayed by the electrostatic surface of Φ11 phage dUTPase, the physiological interaction partner of Stl, whose protein sequence contains an insert region not found in other dUTPase homologues (Fig. S6G), which accounts for the dissimilarity. This difference might also be responsible for the strongest binding, and therefore the most efficient inhibition of the phage dUTPase by Stl.

Together with the kinetic and inhibition data, the conserved active-site engagement observed in the *Dr*DUT–Stl^{NT} structure provides a mechanistic foundation to investigate the potential *in vivo* effects of Stl injection on early zebrafish development.

Figure 2.

2.5 Stl microinjection induces early embryonic lethality in zebrafish

Given the robust *Dr*DUT–Stl interaction and enzyme inhibition demonstrated above, we next investigated the biological consequences of these interactions during early developmental stages (embryogenesis and the beginning of the larval stage) by microinjecting Stl^{WT} into fertilized zebrafish oocytes, as it exerted the highest *in vitro* inhibition of *Dr*DUT. Moreover, we also examined the *in vivo* effect of the Stl^{AA} variant to exclude any possible impact resulting from the DNA-binding ability of the wild-type protein. In addition, we included the Stl^{YAYA} variant as a critical negative control for *Dr*DUT complexation. In line with inability of this mutant to bind to the Φ11 phage dUTPase [16], our *in vitro* experiments demonstrated that this mutant neither binds nor inhibits *Dr*DUT, allowing us to distinguish specific effects of dUTPase inhibition from potential nonspecific effects of protein microinjection. Embryo survival was assessed in multiple biological replicates involving a large number of embryos per experimental condition, and development was monitored throughout early embryogenesis. Direct injection of dUTPase inhibitor proteins in this form might have an immediate functional effect from early

embryonic stages, in contrast to our previous "crispant" dUTPase knockout experiment, where the maternal effect persists until the maternal-to-zygotic transition, as the proteins stored by the mother are still present in the descendants at that point [10]. Both inhibitory Stl variants (Stl^{WT} and Stl^{AA}) markedly reduced embryo survival compared to negative controls (the non-binding, non-inhibitory Stl^{YAYA}-injected, buffer-injected and uninjected controls). By 48 hours post fertilization (hpf), survival in groups injected with Stl^{WT} and Stl^{AA} progressively decreased, it was approximately 60%, whereas ~90% of embryos remained healthy in the controls (Fig. 3). The survival rate was monitored up to 80 hpf, and it was found that the difference between the inhibitory and control groups persisted throughout the entire observation period. By the end of the experiment, the survival rate had decreased further, to approximately 50 % in the Stl^{WT} and 60 % in the Stl^{AA} injected groups. While in the negative control groups injected with the non-binding, non-inhibitory Stl^{YAYA} variant or buffer, and in the uninjected group – the embryos maintained a survival rate of approximately 85-90 %, which showed only a slight reduction compared to the 48 hpf. Figure 3 panels F-I show representative images of zebrafish embryos at 56 hpf microinjected with Stl^{WT}, Stl^{AA}, and Stl^{YAYA} where individuals with morphogenetic defects are marked with asterisks. These developmental abnormalities were mainly observed in the form of structural defects, pericardial and/or yolk sac oedema, and delayed development. These were not protein-specific as they could be seen in all experiments including the uninjected controls, differing only in their frequency, their occurrence was markedly higher in embryos injected with the inhibitory Stl^{WT} and Stl^{AA} variants (Fig. S8). In many affected embryos, multiple abnormalities occurred simultaneously, indicating a general impairment of normal development. Importantly, the low level of lethality or developmental abnormalities observed following Stl^{YAYA} microinjection, was similar to those seen with the buffer and the uninjected embryos, demonstrates that the protein microinjection itself is not responsible for the detected phenotype. Given the similar effects of Stl^{WT} and the DNA-binding-deficient Stl^{AA} variant, these results indicate that the embryonic lethality is specifically caused by the binding and inhibition of dUTPase, rather than by the DNA-binding activity or any other intrinsic property of the Stl protein (Fig. 3A-E).

These experimental results reinforce our previous conclusion derived from the dUTPase crispant knockout screen, namely that dUTPase enzyme is essential for zebrafish development [10]. This difference validates our hypothesis that maternal dUTPase protein is still present in the early stages of development and contributes to embryonic viability.

Figure 3.

3 Discussion

Our results support the essential role of dUTPase activity during early development, consistent with previous studies in *Drosophila melanogaster* and mice that demonstrated early embryonic lethality upon loss of dUTPase[7,9]. The enzyme's essentiality during embryogenesis could be necessary through at least two mechanisms. In the canonical model, dUTPase contributes to the balance in dUTP/dTTP levels. Therefore, it indirectly prevents uracil misincorporation and repair-induced DNA damage [1,32]. In addition, recent work from our laboratory has uncovered a conserved, non-canonical mitotic role for dUTPase, which was published in a bioRxiv preprint. Notably, in *Drosophila* and mouse embryos loss of dUTPase causes early embryonic lethality characterized by severe mitotic failure that cannot be rescued by disabling uracil-DNA repair. These phenotypes include centrosome amplification, spindle defects, and chromosome segregation errors. Together, these observations suggest that a non-canonical mitotic role for dUTPase is conserved from insects to mammals [11].

Our aim was to investigate whether Stl can be used as a molecular tool in eukaryotic cells as a dUTPase inhibitor, as its inhibitory effect has already been demonstrated against dUTPases of various organisms *in vitro* [15,17–21]. For this reason, we first verified that Stl protein also interacts with zebrafish dUTPase. Biophysical measurements revealed high-affinity binding in the nanomolar range and significant thermal stabilization of the *Dr*DUT–Stl complex, suggesting that Stl is able to form stable inhibitory complexes with zebrafish dUTPase under physiological conditions. The determined binding affinity of Stl^{WT} to *Dr*DUT was comparable to that reported for the human dUTPase, but weaker than that determined in the case of *MtDUT* (Table II). Consistent with the binding affinity results, Stl^{WT} showed reduced inhibitory activity against *Dr*DUT compared to hDUT and MtDUT, suggesting species-specific differences in complex formation (Table III). Notably, we observed a difference of approximately two orders of magnitude between the K_D value determined by BLI and the apparent inhibitory constant ($K_{i,app}$) derived from *Dr*DUT activity assays, similarly to differences previously found for the *Mt*DUT-Stl^{WT} interaction [22]. This can presumably be explained, on the one hand, by the fact that during BLI experiments, we examined the Stl^{WT}-*Dr*DUT interaction in a substrate-free environment, and on the other hand, we applied a measurement setup that eliminates the effect of Stl homodimerization, which competes with dUTPase-binding [22,31]. This enabled the determination of the intrinsic binding affinity (dissociation constant) between the proteins, which accordingly suggests a significantly stronger interaction than the $K_{i,app}$ value obtained by the enzyme activity assay. Nevertheless, *in vitro* activity measurements showed approximately 50% inhibition of

*Dr*DUT catalytic activity. Although this indicates only partial inhibition, previous mammalian cell-based studies have shown that even this moderate reduction in dUTPase activity can have biologically significant consequences. This could significantly affect nucleotide homeostasis and cell sensitivity to thymidylate synthase therapies, both in terms of pharmacological inhibition and siRNA-mediated knockdown [33,34].

Our structural data of the *Dr*DUT–Stl^{NT} complex shows that Stl binds to the dUTPase active site and the C-terminal 5th motif arm through a conserved mechanism, thereby sterically blocking the substrate-binding pocket, as observed in other trimeric dUTPase-Stl^{NT} complexes. On the one hand, by blocking the substrate binding site of the enzyme, its canonical function is impaired. On the other hand, as additional dUTPase surfaces are involved in the interaction with Stl, thus potential binding interfaces with mitosis-related partners could be covered. These structural and biochemical findings support a mechanistic model in which the observed binding mode of Stl could potentially influence both processes.

In zebrafish, *Dr*DUT is present at stable levels during early embryogenesis [10,28]. In our present study, *in vivo* microinjection experiments into fertilized eggs showed that wild-type Stl induces severe early developmental defects, leading to high embryo mortality (~40%) within 48 hours after fertilization. Similar phenotypes produced by Stl^{WT} and the DNA-binding-deficient Stl^{AA} variant, together with the lower incidence of developmental abnormalities following microinjection of the non-binding Stl^{YAYA}– as was also the case with microinjection of buffer and uninjected controls – strongly indicates that the detected lethality arises primarily from dUTPase binding and its inhibition, rather than from DNA interaction or nonspecific effects of protein microinjection. We note that the largest effect on embryo survival occurs after 4 hpf, but before 24 hpf. This suggests that injection of Stl isoforms is not toxic, but it interferes with some essential functions during early embryogenesis. One such essential function is the activation of the zygotic genome (ZGA), which incidentally starts right before the 4 hpf timepoint [35,36]. The temporally or spatially impaired activation of zygotic genes often leads to morphological defects. Our data suggest that maternal *Dr*Dut plays a crucial role in the early pre-ZGA cleavage stages, and probably performs crucial house-keeping functions in these earliest stages of development. Its impairment leads to death and morphological defects, also highlighting the importance of dUTPase presence before ZGA.

The ca. 40% lethality rate, measured after 2 days of Stl-mediated inhibition, was only detected approximately 10–12 days after fertilization in *dut* crispant embryos lacking zygotic dUTPase [10]. This delayed death in the case of crispant fish likely reflects the protective effect of maternal

dUTPase, whereas this maternal protein pool is functionally inhibited in Stl microinjected embryos. It is noteworthy that no similar phenotype was observed following the injection of Stl^{YAYA} variant, which is defective in dUTPase binding, further supporting the conclusion that the inhibition of maternal dUTPase activity, rather than the presence of the injected protein itself, is responsible for the accelerated embryonic lethality. Moreover, the phenotype detected following microinjection of Stl^{WT} and Stl^{AA} – in contrast to the absence of a phenotype observed in embryos injected with buffer or Stl^{YAYA} is consistent with the injected inhibitory proteins remaining functionally active *in vivo* long enough to influence dUTPase activity during early embryogenesis.

Based on our current experimental results, we can only distinguish morphological abnormalities and mortality, and do not allow us to determine whether the observed lethality is primarily due to disruption of nucleotide metabolism or impairment of the possible mitotic functions of dUTPase.Therefore, further experiments will be needed to determine the mechanisms causing these effects.

Together, our structural, biochemical and zebrafish *in vivo* data suggest a relationship between dUTPase inhibition and developmental outcome: only those Stl variants that were capable of binding to and inhibiting *Dr*DUT caused embryonic lethality, whereas the phenotype of the non-binding, non-inhibiting Stl^{YAYA} variant was similar to that of the buffer and uninjected controls. These findings establish Stl as an effective protein inhibitor of eukaryotic dUTPase that can perturb dUTPase function during early vertebrate development. Just as UGI has been repurposed from phage defence into a cornerstone of cytosine base editing [37,38], Stl may likewise be adaptable as a modular protein tool for targeted dUTPase perturbation beyond developmental biology. Emerging applications of protein inhibitors *in vivo*, such as antiCRISPR proteins used for tissue specific Cas9 suppression in Drosophila [39] and ribonucleoprotein injections for transient CRISPR–Cas13 activity in zebrafish [40], illustrate how proteinaceous regulators can be deployed for precise, spatiotemporal control of cellular enzymes involved in genome editing and nucleotide metabolism. In an analogous manner, inducible or tissue-specific expression, or refined microinjection [41] of Stl variants, could enable controlled inhibition of dUTPase in defined cell types or developmental windows, providing a versatile platform to interrogate dUTPase functions in diverse eukaryotic systems.

4 Materials and methods

4.1 Cloning and mutagenesis

To generate Stl^{YAYA} mutant from Stl-encoding pGEX-4T-1 vector [15], site-directed mutagenesis was performed using YAYA_F (5'-GCAGCAAGCAGCTATGATCTGTATG-3') and YAYA_R (5'-AATATCGCCATCGTTATAATAC-3') primers. After PCR amplification, the construct was treated with KLD enzyme mix (New England Biolabs), then transformed into *E. coli* XL1Blue strain. The plasmid was purified with NuceloSpin Plasmid CleanUp Kit (Macherey-Nagel) and the sequence was verified by Sanger-sequencing.

4.2 Protein expression and purification

All proteins in this study were expressed in *Escherichia coli* Rosetta strain (Novagen) in LB media. After OD_{600} reached 0.6, protein overexpression was induced with 0.5 mM isopropyl-β-D-thiogalactopyranoside (IPTG). The zebrafish dUTPase (*Dr*DUT (UniProt ID: Q5XJ23 lacking N-terminal 1-26 sequence element)[10] and Stl protein variants (Stl^{WT} (UniProt ID: Q9F0J8)[15], Stl^{AA} [25], Stl^{NT} [22,23] and Stl^{YAYA}[16]) were expressed for 4 hours at 37 °C, and overnight at 18 °C, respectively. Cells were harvested by centrifugation at 4000 rpm for 30 minutes at 4 °C and then washed with PBS. The pellets were lysed by resuspension in lysis buffer (50 mM Tris pH 7.5, 300 mM NaCl, 0.5 mM EDTA, 5 mM benzamidine, 1 mM PMSF, 0.1% (v/v) Triton X-100, 10 mM 2-mercaptoethanol, 10 mg/l DNase, and a half tablet of EDTA-free protease inhibitor (Roche)) and sonication for three 60 s intervals, with 1-minute breaks in between, while the medium was cooled on ice. Afterwards, cell debris was centrifuged at 11000 rpm for 30 minutes at 4 °C. The His-tagged zebrafish dUTPase was purified on Ni-NTA column (Novagen), and the GST-tagged Stl variants were purified on Glutathione Sepharose® 4B column (Cytiva). The purification steps are described in previous work[15]. The Avi-tagged Stl^{WT} used in biolayer interferometry experiments, was purified similarly as the other Stl variant with subtle differences as follows. An overnight cultured and centrifuged AVB101 cell pellet (containing BirA biotin ligase) and 50 mM D-biotin was added to the cell pellet containing the Avi-tagged protein- and lysis buffer, the lysate was incubated at 4°C for 30 min to allow biotinylation of the protein. The purified protein fractions were analyzed by SDS-PAGE. The protein concentration of the samples was estimated by measuring absorbance values at 280 nm using Nanodrop 2000c (Thermo Scientific). Based on the sequences, the extinction coefficients were estimated by ExPASy server [42].

4.3 Differential scanning fluorimetry (Thermofluor)

To determine the stability of the proteins and the interaction of zebrafish dUTPase with different Stl protein constructs, we performed a thermofluorimetric assay. For the 25 µl reaction, 25 µM protein concentrations, with 1000X SYPRO Orange stain, were used in Hard-Shell® 96-Well PCR Plates (Bio-Rad). The measurements were performed using BioRad CFX qPCR device at SYBR channel between 30 °C and 80 °C, rising in 0.5 °C increments. The results were analyzed by using Bio-Rad CFX Maestro software.

4.4 Activity assay

The hydrolysis of dUTP by dUTPase into dUMP and PPi releases protons, which were continuously monitored in phenol red-containing activity buffer (1 mM HEPES pH 7.5, 5 mM $MgCl_2$, 150 mM KCl, 40 µM Phenol Red indicator) at 559 nm using a Jasco V550 spectrophotometer. After 5 minutes of pre-incubation of 50 nM *Dr*DUT and variable concentrations of Stl protein variants at 25 °C, the reaction was initiated by adding 30 µM dUTP. From the first 10% of the progression curve, the initial velocity was determined. To define the apparent inhibitory constant (K_i), the Stl inhibition data were fitted to a quadratic binding equation [21] using OriginPro 2018 software (OriginLab Corporation).

4.5 Biolayer interferometry

Binding kinetics analysis between Stl^{WT} and *Dr*DUT was performed using biolayer interferometry. Measurements were carried out utilizing an Octet K2 system (FortéBio) with high-precision streptavidin biosensors at 30 °C. Biotinylated Avi-tagged Stl^{WT} was immobilized onto the biosensors at 68 µg/ml concentration after equilibration and determination of baseline in buffer A (50 mM HEPES pH 7.5, 300 mM NaCl, 5 mM $MgCl_2$). Experimental conditions were set using Octet Data Acquisition software, and data analysis and calculation of kinetic parameters were performed using Octet Data Analysis software.

4.6 Zebrafish husbandry and microinjections

Wild-type AB strain zebrafish were maintained and bred in the fish facility of the Biology Institute of ELTE Eötvös Loránd University, according to standard protocols of the field [43,44]. Embryos were raised in E3 medium (5 mM NaCl, 0.17 mM KCl, 0.33 mM $CaCl_2$, and 0.33 mM $MgSO_4$ in distilled water) in a 28.5 ºC incubator. 2 nl of Stl buffer (50 mM Tris pH 7.5, 300 mM NaCl, 5 mM $MgCl_2$) or one of the purified proteins (Stl^{WT}, Stl^{AA}, and Stl^{YAYA}) at 1 mg/ml

concentration was injected into embryos at 1-2 cell stage, resulting in final concentration of 300 nM of the inhibitor. Survival was monitored under a stereo microscope.

Experiments described in this paper were carried out in accordance with the Hungarian Act of Animal Care and Experimentation (1998, XXVIII) and with the directive 2010/63/EU of the European Parliament and of the Council of 22 September 2010 on the protection of animals used for scientific purposes. All protocols and experimental procedures used in this work were approved by the Hungarian National Feed Chain Safety Office (PEI/001/1713-2/2015) and the ELTE Eötvös Loránd University, Faculty of Science Animal Welfare Commission.

4.7 Protein crystallization

*Dr*DUT-Stl^{NT} complex was concentrated to 243 μM for crystallization. Sitting drop vapour diffusion crystallization trials were performed, whereby 1 μl of protein solution was mixed with 1 μl of reservoir solution in MRC 48-well crystallization plates (Molecular Dimensions). Crystals appeared in a condition containing 10 % w/v PEG 4000, 0.1 M Sodium HEPES pH 7.0, 10 % v/v 2-Propanol, and were cryoprotected in oil (LV CryoOil, MiTeGen), prior to flash freezing in liquid nitrogen.

4.8 Crystal data collection and structure determination

X-ray diffraction data were collected at 100 K at the IO3 beamline of the Diamond Light Source Synchrotron at 0.9763 Å wavelength. Data were indexed, integrated, and scaled using the *DIALS* pipeline (v. 3.17.0-1) implemented at Diamond Light Source [45]. The structure was determined by molecular replacement using the human dUTPase (PDB: 2HQU) and *S. aureus* Stl (PDB: 7PWJ) as search models in Phaser. Model building and refinement were carried out in PHENIX (version1.20.1_4487), with a first round of automated model building performed by the AutoBuild wizard [46] followed by iterative rounds of model building with WinCoot (v.0.9.6) [47] and refinement using phenix.refine. There are two essentially identical heterohexamer complexes in the asymmetric unit, each comprising a *Dr*DUT trimer complexed with three Stl^{NT}. The data collection and refinement statistics are presented in (Table S2) with favoured Ramachandran values of 99.27% and no outliers.

4.9 Protein-protein interaction analysis

The analysis of intermolecular interactions of *Dr*DUT-Stl^{NT} complex crystal structure (PDB ID: 9TRU) and the surface area of dUTPase-Stl^{NT} interfaces was carried out using PDBePISA (https://www.ebi.ac.uk/pdbe/pisa/pistart.html) [48] software.

4.10 Protein structure prediction

The 3D structures of Stl^{WT,} Stl^{AA} and Stl^{YAYA} were predicted with AlphaFold 3 [49] (https://alphafoldserver.com). In each case 5-5 models were generated using the protein sequences of Stl^{WT} (UniProt: Q9F0J8), and the StlWT sequence containing the double mutations (Q40A,Q41A for Stl^{AA} and Y112A,Y113A for Stl^{YAYA}).

4.11 Software used in creation of figures

The illustrations of crystal structures and AlphaFold models were created using PyMOL (ver. 3.1.4.1, Schrodinger, LLC), electrostatic potential molecular surfaces were created utilizing APBS Electrostatics plugin [50]. BLI graph was created using Octet Data Analysis software (FortéBio), other graphs were made using Origin 2018 and Excel (Microsoft 365, Microsoft Corporation). The illustrations and final figures from individual graphs were created with Corel 2020 (Corel Corporation) and PowerPoint (Microsoft 365, Microsoft Corporation).

Acknowledgement

This work was supported by the National Research, Development and Innovation Fund of Hungary (PD134324 to KN and K146890, 2025-1.2.7-HU-CN-PARTNER-2025-00025 to BGV), and the ICGEB Research Grants Programme 2023 (CRP/HUN23-02). MV was also supported by the ÚNKP-22-5 New National Excellence Program of the Ministry of Culture and Innovation from the source of the National Research, Development and Innovation Fund. MV, KN and GNN are both János Bolyai fellows of the Hungarian Academy of Sciences. GNN gratefully acknowledges the support of the Mihály Somogyi Grant of the Varga József Foundation. KN gratefully acknowledges the support of the Hungarian Academy of Sciences provided for scientists raising young children.

We would like to thank Anita Rácz for fish care.

Author contributions

Study design: VPS, ZST, GNN, BGV, KN

Performed experiments: VPS, ZST, DD, LK

Interpreted data: VPS, ZST, LK, MV, GNN, BGV, KN

Wrote article: VPS, ZST, MV, GNN, BGV, KN

Data and materials availability: The atomic coordinates and structure factors have been deposited in the Protein Data Bank with access code 9TRU. All data needed to evaluate the conclusions in the paper are present in the paper and/or the Supplementary Materials. Additional data related to this paper may be requested from the authors.

Competing financial interest statement

The authors declare that they have no conflict of interest.

References

1. Vértessy BG, Tóth J (2009) Keeping uracil out of DNA: physiological role, structure and catalytic mechanism of dUTPases. Acc. Chem. Res. 42:97–106.

2. Szabó JE, Takács E, Merényi G, Vértessy BG, Tóth J (2016) Trading in cooperativity for specificity to maintain uracil-free DNA. Sci. Rep. 6:24219.

3. Nagy GN, Leveles I, Vértessy BG (2014) Preventive DNA repair by sanitizing the cellular (deoxy)nucleoside triphosphate pool. FEBS J. 281:4207–4223.

4. Takács E, Grolmusz VK, Vértessy BG (2004) A tradeoff between protein stability and conformational mobility in homotrimeric dUTPases. FEBS Lett. 566:48–54.

5. Dengg M, Garcia-Muse T, Gill SG, Ashcroft N, Boulton SJ, Nilsen H (2006) Abrogation of the CLK-2 checkpoint leads to tolerance to base-excision repair intermediates. EMBO Rep. 7:1046–1051.

6. Castillo-Acosta VM, Estévez AM, Vidal AE, Ruiz-Perez LM, González-Pacanowska D (2008) Depletion of dimeric all-alpha dUTPase induces DNA strand breaks and impairs cell cycle progression in Trypanosoma brucei. Int. J. Biochem. Cell Biol. 40:2901–2913.

7. Muha V, Horváth A, Békési A, Pukáncsik M, Hodoscsek B, Merényi G, Róna G, Batki J, Kiss I, Jankovics F, et al. (2012) Uracil-containing DNA in Drosophila: stability, stage-specific accumulation, and developmental involvement. PLoS Genet. 8:e1002738.

8. Siaud N, Dubois E, Massot S, Richaud A, Dray E, Collier J, Doutriaux M-P (2010) The SOS screen in Arabidopsis: a search for functions involved in DNA metabolism. DNA Repair (Amst) 9:567–578.

9. Pálinkás HL, Rácz GA, Gál Z, Hoffmann OI, Tihanyi G, Róna G, Gócza E, Hiripi L, Vértessy BG (2019) CRISPR/Cas9-Mediated Knock-Out of dUTPase in Mice Leads to Early Embryonic Lethality. Biomolecules 9.

10. Perey-Simon V, Békesi A, Kazzazy L, Mihály J, Varga M, Vértessy BG, Nyíri K (2025) dUTPase is essential in zebrafish development and possesses several single-nucleotide variants with pronounced structural and functional consequences. FEBS Open Bio.

11. Nagy N, Tóth O, Oláh E, Henn L, Rácz GA, Szabó E, Várady G, Vigh FB, Golács ZR, Urbán M, et al. (2026) Recognizing dUTPase as a mitotic factor essential for early embryonic development. BioRxiv.

12. Mol CD, Arvai AS, Sanderson RJ, Slupphaug G, Kavli B, Krokan HE, Mosbaugh DW, Tainer JA (1995) Crystal structure of human uracil-DNA glycosylase in complex with a protein inhibitor: protein mimicry of DNA. Cell 82:701–708.

13. Komor AC, Zhao KT, Packer MS, Gaudelli NM, Waterbury AL, Koblan LW, Kim YB, Badran AH, Liu DR (2017) Improved base excision repair inhibition and bacteriophage Mu Gam protein yields C:G-to-T:A base editors with higher efficiency and product purity. Sci. Adv. 3:eaao4774.

14. Davidson AR, Lu W-T, Stanley SY, Wang J, Mejdani M, Trost CN, Hicks BT, Lee J, Sontheimer EJ (2020) Anti-CRISPRs: Protein Inhibitors of CRISPR-Cas Systems. Annu. Rev. Biochem. 89:309–332.

15. Szabó JE, Németh V, Papp-Kádár V, Nyíri K, Leveles I, Bendes AÁ, Zagyva I, Róna G, Pálinkás HL, Besztercei B, et al. (2014) Highly potent dUTPase inhibition by a bacterial repressor protein reveals a novel mechanism for gene expression control. Nucleic Acids Res. 42:11912–11920.

16. Ciges-Tomas JR, Alite C, Humphrey S, Donderis J, Bowring J, Salvatella X, Penadés JR, Marina A (2019) The structure of a polygamous repressor reveals how phage-inducible chromosomal islands spread in nature. Nat. Commun. 10:3676.

17. Hirmondó R, Szabó JE, Nyíri K, Tarjányi S, Dobrotka P, Tóth J, Vértessy BG (2015) Cross-species inhibition of dUTPase via the Staphylococcal Stl protein perturbs dNTP pool and colony formation in Mycobacterium. DNA Repair (Amst) 30:21–27.

18. Benedek A, Pölöskei I, Ozohanics O, Vékey K, Vértessy BG (2018) The Stl repressor from Staphylococcus aureus is an efficient inhibitor of the eukaryotic fruitfly dUTPase. FEBS Open Bio 8:158–167.

19. Wang F, Liu C, Wang C, Wang Y, Zang K, Wang X, Liu X, Li S, Li F, Ma Q (2021) Structural basis of staphylococcal Stl inhibition on a eukaryotic dUTPase. Int. J. Biol. Macromol. 184:821–830.

20. Nyíri K, Mertens HDT, Tihanyi B, Nagy GN, Kőhegyi B, Matejka J, Harris MJ, Szabó JE, Papp-Kádár V, Németh-Pongrácz V, et al. (2018) Structural model of human dUTPase in complex with a novel proteinaceous inhibitor. Sci. Rep. 8:4326.

21. Benedek A, Temesváry-Kis F, Khatanbaatar T, Leveles I, Surányi ÉV, Szabó JE, Wunderlich L, Vértessy BG (2019) The Role of a Key Amino Acid Position in Species-Specific Proteinaceous dUTPase Inhibition. Biomolecules 9.

22. Tóth ZS, Leveles I, Nyíri K, Nagy GN, Harmat V, Jaroentomeechai T, Ozohanics O, Miller RL, Álvarez MB, Vértessy BG, et al. (2024) The homodimerization domain of the Stl repressor is crucial for efficient inhibition of mycobacterial dUTPase. Sci. Rep. 14:27171.

23. Kőhegyi B, Tóth ZS, Gál E, Laczkovich M, Benedek A, Vértessy BG, Nyíri K (2025) Full-length inhibitor protein is the most effective to perturb human dUTPase activity. Sci. Rep. 15:4836.

24. Sanz-Frasquet C, Ciges-Tomas JR, Alite C, Penadés JR, Marina A (2023) The Bacteriophage-Phage-Inducible Chromosomal Island Arms Race Designs an Interkingdom Inhibitor of dUTPases. Microbiol. Spectr. 11:e0323222.

25. Nyíri K, Kőhegyi B, Micsonai A, Kardos J, Vertessy BG (2015) Evidence-Based Structural Model of the Staphylococcal Repressor Protein: Separation of Functions into Different Domains. PLoS ONE 10:e0139086.

26. Pecsi I, Hirmondo R, Brown AC, Lopata A, Parish T, Vertessy BG, Tóth J (2012) The dUTPase enzyme is essential in Mycobacterium smegmatis. PLoS ONE 7:e37461.

27. Hirmondo R, Lopata A, Suranyi EV, Vertessy BG, Toth J (2017) Differential control of dNTP biosynthesis and genome integrity maintenance by the dUTPase superfamily enzymes. Sci. Rep. 7:6043.

28. da Silva Pescador G, Baia Amaral D, Varberg JM, Zhang Y, Hao Y, Florens L, Bazzini AA (2024) Protein profiling of zebrafish embryos unmasks regulatory layers during early embryogenesis. Cell Rep. 43:114769.

29. Abrams EW, Mullins MC (2009) Early zebrafish development: it's in the maternal genes. Curr. Opin. Genet. Dev. 19:396–403.

30. Wang Y, Wang X, Wang W, Cao Z, Zhang Y, Liu G (2024) Screening of functional maternal-specific chromatin regulators in early embryonic development of zebrafish. Commun. Biol. 7:1354.

31. Nyíri K, Gál E, Laczkovich M, Vértessy BG (2024) Antirepressor specificity is shaped by highly efficient dimerization of the staphylococcal pathogenicity island regulating repressors: Stl repressor dimerization perturbed by dUTPases. Sci. Rep. 14:1953.

32. Nyman PO (2001) Introduction. dUTPases. Curr. Protein Pept. Sci. 2:277–285.

33. Wilson PM, LaBonte MJ, Lenz H-J, Mack PC, Ladner RD (2012) Inhibition of dUTPase induces synthetic lethality with thymidylate synthase-targeted therapies in non-small cell lung cancer. Mol. Cancer Ther. 11:616–628.

34. Yano W, Yokogawa T, Wakasa T, Yamamura K, Fujioka A, Yoshisue K, Matsushima E, Miyahara S, Miyakoshi H, Taguchi J, et al. (2018) TAS-114, a First-in-Class Dual dUTPase/DPD Inhibitor, Demonstrates Potential to Improve Therapeutic Efficacy of Fluoropyrimidine-Based Chemotherapy. Mol. Cancer Ther. 17:1683–1693.

35. Kazzazy L, Mező D, Nagy KK, Perey-Simon V, Tóth J, Békési A, Vértessy B, Varga M (2025) Noncanonical Nucleotides in the Genome Around the Maternal-Zygotic Transition. J. Exp. Zool. B Mol. Dev. Evol.

36. Akdogan-Ozdilek B, Duval KL, Goll MG (2020) Chromatin dynamics at the maternal to zygotic transition: recent advances from the zebrafish model. F1000Res. 9.

37. Shi Z, Cheng T-L (2025) UGI relocation inside Cas9 reduces Cas9 dependent off target effects in cytosine base editors. Sci. Rep. 15:35518.

38. Hess GT, Tycko J, Yao D, Bassik MC (2017) Methods and Applications of CRISPR-Mediated Base Editing in Eukaryotic Genomes. Mol. Cell 68:26–43.

39. Viswanatha R, Entwisle S, Hu Y, Kim A-R, Reap K, Butnaru M, Qadiri M, Mohr SE, Perrimon N (2025) Higher resolution pooled genome-wide CRISPR knockout screening in Drosophila cells using integration and anti-CRISPR (IntAC). Nat. Commun. 16:6498.

40. Moreno-Sánchez I, Hernández-Huertas L, Nahón-Cano D, Martínez-García PM, Treichel AJ, Gómez-Marin C, Tomás-Gallardo L, da Silva Pescador G, Kushawah G, Egidy R, et al. (2025) Enhanced RNA-targeting CRISPR-Cas technology in zebrafish. Nat. Commun. 16:2591.

41. Abdelrahman D, Hasan W, Da'as SI (2021) Microinjection quality control in zebrafish model for genetic manipulations. MethodsX 8:101418.

42. Wilkins MR, Gasteiger E, Bairoch A, Sanchez JC, Williams KL, Appel RD, Hochstrasser DF (1999) Protein identification and analysis tools in the ExPASy server. Methods Mol. Biol. 112:531–552.

43. Westerfield M The zebrafish book: A guide for the laboratory use of zebrafish (Danio rerio). 4th ed. Eugene, OR, USA: University of Oregon Press; 2000.

44. Aleström P, D'Angelo L, Midtlyng PJ, Schorderet DF, Schulte-Merker S, Sohm F, Warner S (2020) Zebrafish: Housing and husbandry recommendations. Lab. Anim. 54:213–224.

45. Winter G, Waterman DG, Parkhurst JM, Brewster AS, Gildea RJ, Gerstel M, Fuentes-Montero L, Vollmar M, Michels-Clark T, Young ID, et al. (2018) DIALS: implementation and evaluation of a new integration package. Acta Crystallogr. D Struct. Biol. 74:85–97.

46. Terwilliger TC, Grosse-Kunstleve RW, Afonine PV, Moriarty NW, Zwart PH, Hung LW, Read RJ, Adams PD (2008) Iterative model building, structure refinement and density modification with the PHENIX AutoBuild wizard. Acta Crystallogr. D Biol. Crystallogr. 64:61–69.

47. Emsley P, Lohkamp B, Scott WG, Cowtan K (2010) Features and development of *Coot*. Acta Crystallogr. D Biol. Crystallogr. 66:486–501.

48. Krissinel E, Henrick K (2007) Inference of macromolecular assemblies from crystalline state. J. Mol. Biol. 372:774–797.

49. Abramson J, Adler J, Dunger J, Evans R, Green T, Pritzel A, Ronneberger O, Willmore L, Ballard AJ, Bambrick J, et al. (2024) Accurate structure prediction of biomolecular interactions with AlphaFold 3. Nature 630:493–500.

50. Jurrus E, Engel D, Star K, Monson K, Brandi J, Felberg LE, Brookes DH, Wilson L, Chen J, Liles K, et al. (2018) Improvements to the APBS biomolecular solvation software suite. Protein Sci. 27:112–128.

Tables

Table I. Thermal stability of *Dr*DUT, Stl variants and *Dr*DUT–Stl complexes

	T_m^* (°C)	
	Individual proteins	***Dr*DUT + Stl variant**
***Dr*DUT**	42.7 ± 0.3	-
Stl^{WT}	50.7 ± 0.2	57.3 ± 0.3
Stl^{NT}	52.7 ± 1.3	60.0 ± 0.3
Stl^{AA}	50.7 ± 0.3	57.3 ± 0.4
Stl^{YAYA}	56.7 ± 0.3	43.0 ± 0.3 56.5 ± 0.9

*Average and standard deviation of three technical replicates.

Table II. BLI kinetics of Stl^{WT} -dUTPase binding

Ligand	Analyte	K_D (nM)	k_a (M^{-1} s^{-1}) (10^5)	k_{dis} (s^{-1}) (10^{-5})	χ^2	Ref.
Stl^{WT}-Avi	*Dr*DUT	0.70±0.015	0.69±0.00	4.86±0.10	0.32	this work
Stl^{WT}-Avi	hDUT	0.18±0.001	15.3±0.0	27.3±0.3	1.20	[23,31]
Stl^{WT}-Avi	*Mt*DUT	<0.001	2.70±0.01	<0.01	0.19	[22]

Table III. Inhibition of *Dr*DUT catalytic activity by Stl variants

	Inhibition (%)*	$K_{i,app}$ **(nM)**	***Ref.***
Stl^{WT}-*Dr*DUT	49.6 ± 2.5	41.1 ± 5.9	this work
Stl^{AA}-*Dr*DUT	41.5 ± 2.7	78.5 ± 13.7	this work
Stl^{NT}-*Dr*DUT	35.4 ± 2.8	117.9 ± 28.7	this work
Stl^{YAYA}-*Dr*DUT	0	-	this work
Stl^{WT}-hDUT	~ 70	6.7 ± 2.4	[20]
Stl^{WT}-MtDUT	82 ± 3	2.0 ± 1.2	[22]

*At 400 nM inhibitor concentration

Figures

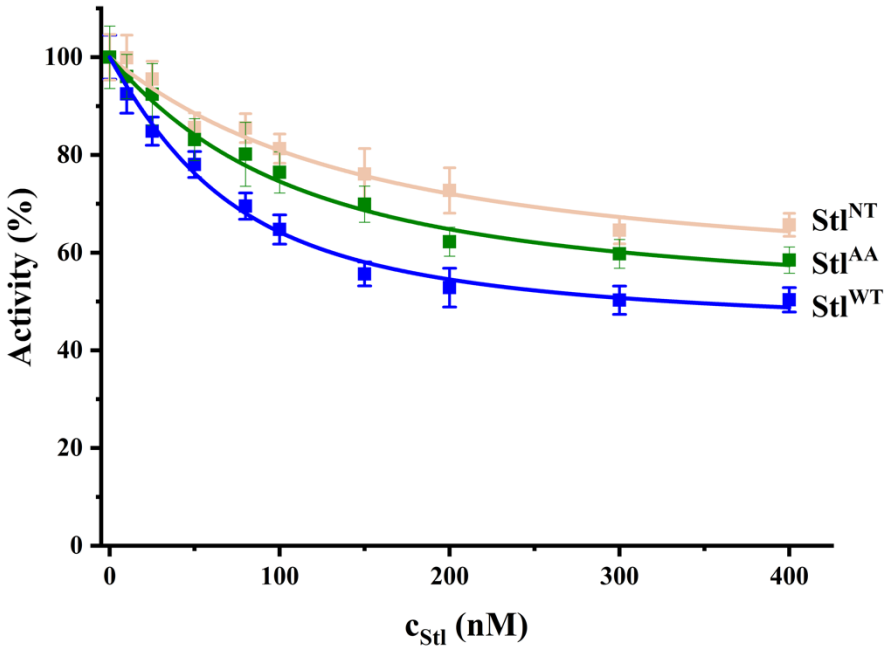

Figure 1. Inhibition of *Dr*DUT catalytic activity by Stl variants. Enzyme activity is expressed as a percentage relative to uninhibited *Dr*DUT. Data were fitted to a quadratic binding equation to determine apparent inhibitory constants: $K_{i,app}$ (Table III). Values represent means ± standard deviations from at least three independent measurements.

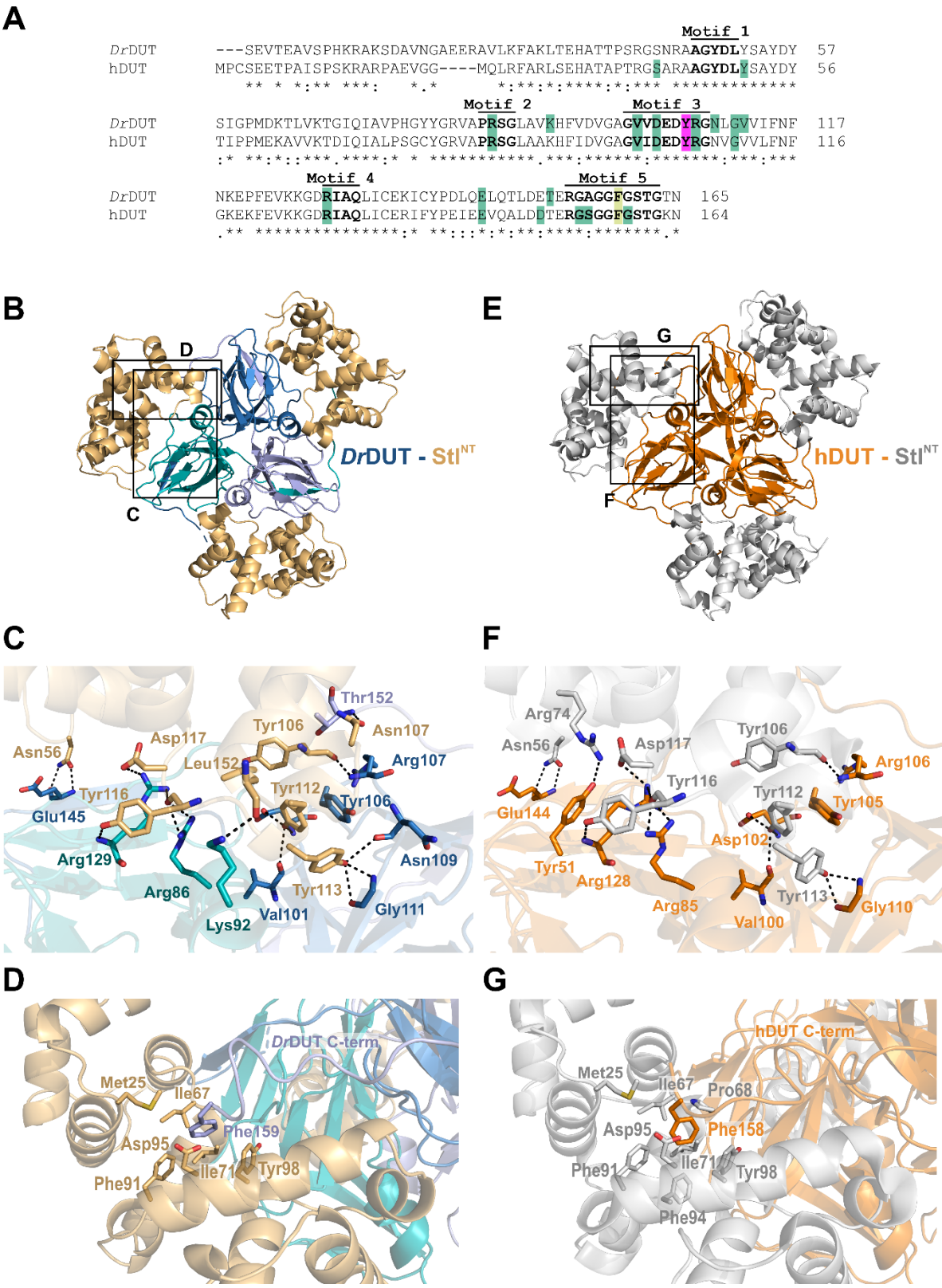

Figure 2. Conserved structural basis of dUTPase inhibition by Stl in zebrafish and human.

(**A**) Sequence alignment of *Danio rerio* (*Dr*DUT) and human (hDUT) dUTPases. Conserved motifs are shown in bold; Stl^{NT}-interacting residues identified from crystal structures (9TRU,

8C8I, 7PWJ, 7DLV) are highlighted in teal (polar interactions), pink (π–π stacking), and light green (motif 5 Phe interactions with the apolar pocket of Stl^{NT}). (**B**) Overall structure of the *Dr*DUT–Stl^{NT} complex. The *Dr*DUT trimer is shown as cartoon with three protomers in different shades of blue; Stl^{NT} is shown in beige. (**C**) Primary binding interface of Stl^{NT} and *Dr*DUT. Interacting residues are shown as sticks with atomic colouring (C as cartoon, N dark blue, O red); H-bonds and salt bridges are shown as black dashed lines. (**D**) Secondary binding site of the *Dr*DUT–Stl^{NT} complex, formed by insertion of the *Dr*DUT C-terminal arm into the apolar pocket of Stl^{NT}. *Dr*DUT Phe159 and pocket-forming Stl^{NT} residues are shown as sticks (C as cartoon, N dark blue, O red, S yellow). (**E)** Overall structure of the hDUT–Stl^{NT} complex (PDB 7PWJ), shown for comparison with panel B. The hDUT trimer is in orange; Stl^{NT}s in grey. (**F)** Primary binding interface of Stl^{NT} and hDUT, shown for comparison with panel C. (**G**) Secondary binding site of the hDUT–Stl^{NT} complex, showing hDUT Phe158 inserted into the apolar pocket of Stl^{NT}, shown for comparison with panel D.

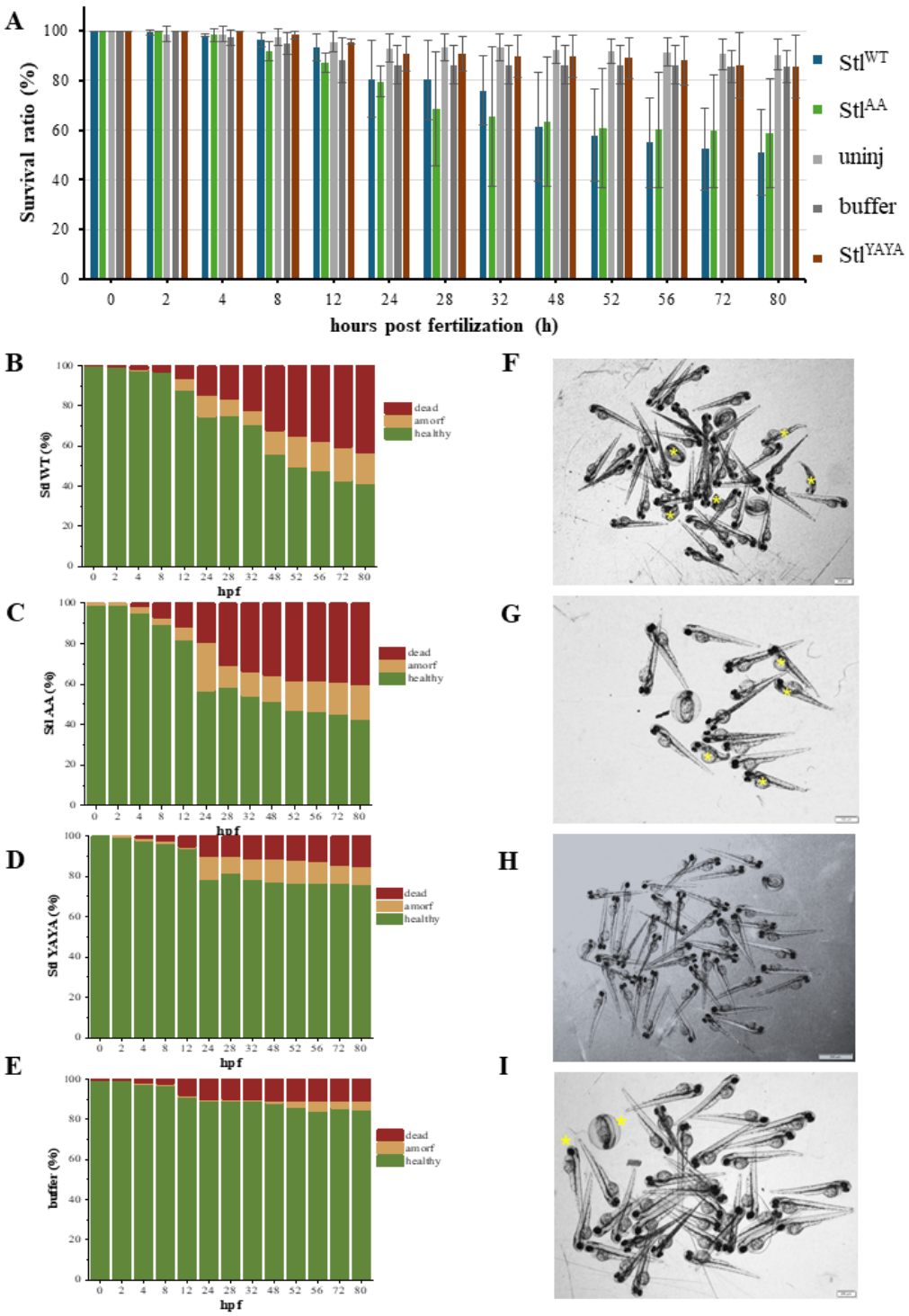

Figure 3. Stl microinjection induces early embryonic lethality in zebrafish. A) Bar chart showing the percentage of surviving embryos. Stl^{WT} is marked in blue, Stl^{AA} in green, the buffer-injected control in dark grey, the uninjected control in light grey, and the Stl^{YAYA} no-binding control in burgundy. **B-E)** Bar charts showing the percentage of embryos that are healthy (green), morphologically abnormal (yellow), or dead (red) at the indicated time points

for Stl^{WT} (**B**), Stl^{AA} (**C**), Stl^{YAYA} (**D**) and buffer (E). At least three independent experiments were performed for each protein. **F–I)** Representative microscopic images of embryos at 56 hpf injected with Stl^{WT} (**F**), Stl^{AA} (**G**), Stl^{YAYA} (**H**) or buffer (I). Embryos with morphogenetic defects are marked with an asterisk.